Geoscience Letters

RESEARCH LETTER

Open Access

Tidal asymmetry and transition in the Singapore Strait revealed by GNSS interferometric reflectometry

Dongju Peng[1*], Kit Ying Soon[2], Victor H. S. Khoo[3], Evert Mulder[3], Poh Weng Wong[3] and Emma M. Hill[1,2]

Abstract

The Singapore Strait is located at the transition between the dominantly semidiurnal Indian Ocean and the mixed-to-diurnal South China Sea, resulting in complex tidal dynamics. In this work, we use sea-level estimates from two coastal Global Navigation Satellite Systems (GNSS) stations and one tide gauge to study tides and tidal asymmetry in the Strait. We first generate sea-level measurements from GNSS signal-to-noise ratio (SNR) data using the GNSS Interferometric Reflectometry technique, which can estimate sea-surface heights from a coastal GNSS station. Second, we perform tidal harmonic analysis and quantify tidal asymmetry based on the skewness method. Finally, we examine seasonal sea-level changes in the Strait from GNSS SNR data, tide-gauge records and satellite altimetry. Our results reveal an increase in M2 and S2 amplitudes toward the west of the Strait and a decrease in the K1 and O1 amplitudes. Our results also show that tides at the two sites in the east are ebb dominant with asymmetry originating from the O1–K1–M2 triad by astronomical forcing, whereas tidal asymmetry at the site in the west is flood dominant and mainly caused by non-linear interaction of the major tidal constituents. Analysis of seasonal sea-level changes shows that annual amplitudes in the east are around 13.6 cm, and 6.7 cm in the west. A possible explanation for the discrepancy in the amplitudes is the effect of seasonal monsoon winds flowing from the South China Sea.

Keywords GNSS-IR, Sea level, Tides, Tidal asymmetry, Seasonal cycle

Introduction

The Singapore Strait (Fig. 1a) is located between two oceans: the Indian Ocean to the West and the Pacific Ocean to the East. It is strongly affected by the different dynamics of these ocean basins. On its Eastern side it connects to the South China Sea, which experiences predominantly diurnal tides associated with the Pacific Ocean. The Western side connects to the Indian Ocean, though the Malacca Strait, which has predominantly semidiurnal tides. The transition from diurnal tides to semidiurnal tides in a shallow (water depth varying from a few meters to 100 m) and narrow (16 km wide and 105 km long) channel results in complex tidal dynamics. In addition, seasonal monsoon winds induce an annual cycle of water-level oscillations (Tay et al. 2016; Tkalich et al. 2013a, b); these oscillations will interact with tidal currents and further add to the complexity of the tidal regime. Such complexities can affect vessel transit times. The Singapore Strait is a crucial gateway between Asia and Europe. It requires a tight traffic management system to ensure that vessels are coming into port at the right time, every time. Furthermore, tides influence the vegetative development of mangrove coasts (Collins et al. 2017), the suspension, transportation, and deposition of sediment (Mitra and Kumar 2021; Molinas et al. 2020; Olliver et al. 2020), and the erosion of shorelines (Vousdoukas

*Correspondence:
Dongju Peng
djpeng@ntu.edu.sg
[1] Earth Observatory of Singapore, Nanyang Technological University, Singapore, Singapore
[2] Asian School of the Environment, Nanyang Technological University, Singapore, Singapore
[3] Singapore Land Authority, Singapore, Singapore

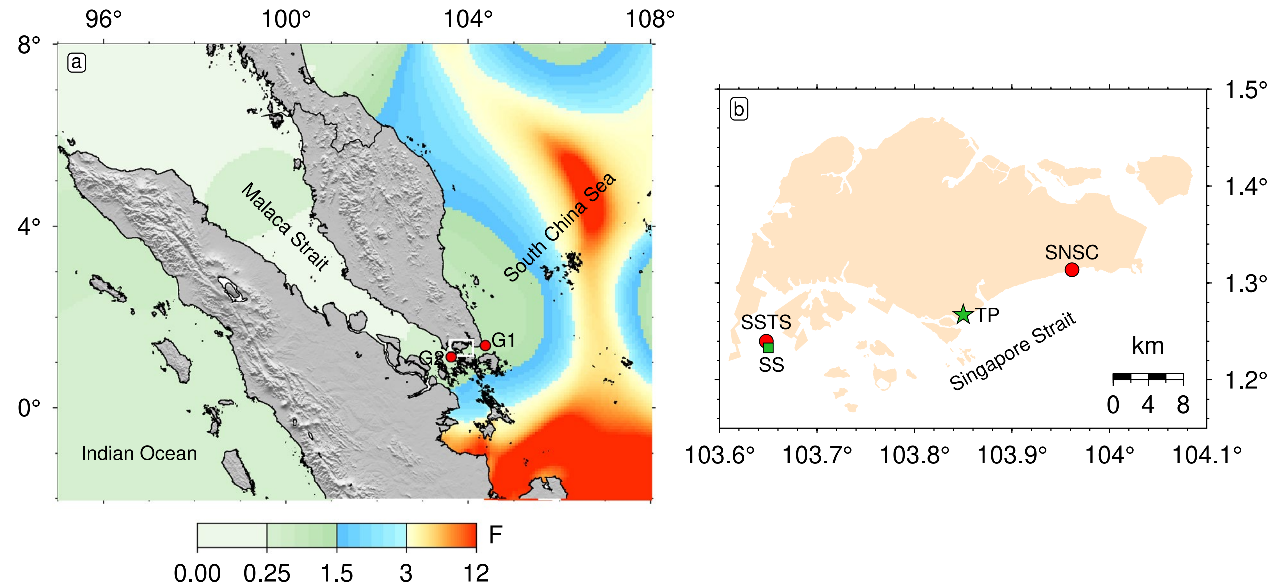

Fig. 1 **a** Geographic locations of our study area (white rectangle) and the two grid points (*G1* and G2) of the satellite altimetry product which are the nearest to GNSS stations SNSC and SSTS in **b**. Color map represents tidal form factor, which is defined by the ratio of the amplitudes of the two main diurnal and semidiurnal constituents (K_1,O_1, M_2 and S_2), $F = \left(A_{K_1} + A_{O_1}\right) / \left(A_{M_2} + A_{S_2}\right)$. The amplitudes used to make this map were taken from the Oregon State University TPXO8-atlas global tide model. Tidal forms are classified as follows: $0 < F < 0.25$, semidiurnal; $0.25 < F < 1.5$, mixed and mainly semidiurnal; $1.5 < F < 3.0$, mixed and mainly diurnal; $F > 3.0$, diurnal. **b** Geographic locations of the two GNSS stations (SNSC and SSTS) and two tide gauges with hourly (TP) and monthly (SS) records publicly available

et al. 2020). Therefore, it is of importance both societally and scientifically to understand the characteristics of tides in the Singapore Strait.

Van Maren and Gerritsen (2012) and Hasan et al. (2016) numerically reproduced the tidal dynamics of Singapore's coastal waters through hydrodynamic modelling of the eight major tidal constituents (M_2, S_2, K_2, N_2, K_1, O_1, P_1, Q_1,). Van Maren and Gerritsen (2012) found that the tides around Singapore are asymmetric due to the interaction of the diurnal constituents with the semidiurnal M_2 tide. Hasan et al. (2016) compared four model setups with tide-gauge observations and revealed that no model performs the best in reproducing both water level and flow velocity simultaneously. In addition, they found that different techniques to quantify model accuracy are inconsistent in determining which model is more accurate because of the complex tidal dynamics around Singapore, where the dominantly tidal currents are decoupled from the semi-diurnal water level oscillations. This implies that more advanced numerical modelling together with denser in-situ observations for capturing the spatial variability of tides are required to fully reproduce the tidal dynamics in Singapore waters. Both studies used real observations of water levels at two to four sites to validate their models; however, only one of the sites is located in the Singapore Strait. Considering the complexity in tides and shoreline geometry in the Strait, more in-situ data are necessarily useful to deepen our understanding of the tidal characteristics and potentially better constrain numerical modelling of tides in the area. In addition, besides estimating the eight major tidal constituents that could be reproduced by numerical modelling, shallow-water tides (which are generated as a result of non-linear effects in shallowing coastal waters and could result in tidal distortion and asymmetry) can be estimated using in-situ data.

Tidal asymmetry usually refers to unequal durations of rising and falling tides, as well as a difference in the duration and magnitude of flooding and ebbing currents (Pugh and Woodworth 2014). Specifically, a shorter duration of the rising tide indicates a flood dominant tidal asymmetry, and a shorter duration of falling tide indicates an ebb-dominant tidal asymmetry. As tidal asymmetry plays a key role in sediment transport and large-scale morphological evolution (De Swart and Zimmerman 2009), it has been intensively studied. Previous studies revealed that tidal asymmetry could originate from astronomical tides alone or the interactions between tides and shallow water bathymetry/shoreline geometry (Jewell et al. 2012; Mandal et al. 2020; Nidzieko 2010). Most of the previous studies were based on conventional tide-gauge observations. Over the past decade, however, a geodetic Global Navigation Satellite System (GNSS) station placed at the coast has been emerging as an in-situ sea-level observing system with comparable accuracy as a conventional tide gauge (Jin et al. 2017; Larson et al. 2013, 2017). Two GNSS stations at the coast of the Singapore Strait that were originally installed for survey purposes can be used as an in-situ sea-level observing system via the GNSS interferometric reflectometry (GNSS-IR) technique, and they are strategically located in the east and west of the Strait, thus potentially capturing the transition of tides in the Strait.

GNSS-IR for measuring water levels uses GNSS satellite signals reflected off the nearby water surface that are delayed with respect to the direct satellite signals (Larson et al. 2013). These reflected signals cause measurable interference in the form of an oscillation of the recorded signal-to-noise ratio (SNR) data at low elevation angles. By analyzing the frequency of the SNR oscillation, we can estimate the vertical distances from the water surface to the GNSS antenna phase center, which are anti-correlated with relative sea-level changes. GNSS-IR has been proven to be effective for detecting astronomical tides with comparable accuracy as conventional tide gauges (Larson et al. 2017; Tabibi et al. 2020). In this study, we aim to (1) improve understanding of tidal transition and characterize tidal asymmetry in the Singapore Strait using observations from two coastal GNSS stations complemented with hourly tide-gauge records, and (2) examine monsoon-driven seasonal sea-level changes in the Strait using GNSS-IR observations, tide-gauge records and satellite altimetry data.

Data and methods

Data

The Singapore Satellite Positioning Reference Network (SiReNT) is the national reference network infrastructure in Singapore. It is developed as an initiative by the Singapore Land Authority to support real-time high-quality positioning, navigation, and tracking. SiReNT consists of nine GNSS reference stations; two of them—SNSC and SSTS—were installed near the coastline (geographic locations are illustrated in Fig. 1b, and photographs in Additional file 1: Figure S1). The GNSS antennas at those two stations receive both direct signals from the GNSS satellites and the reflected signals from the nearby sea surface, so we can use their data to derive sea-level changes. For SNSC, we use 1-Hz SNR data from February 2017 to 2019 due to a change of the antenna model. For SSTS, we use 1-Hz SNR data from 2016 to 2019 because of incomplete data in 2015.

There are 13 tide gauges in Singapore and at one of the sites—Tanjong Pagar (TP in Fig. 1b, acoustic gauge)—hourly tide-gauge records are publicly available. We, therefore, include data at this site for tidal analysis and comparison with GNSS-IR measurements. In addition, another tide gauge at Sultan Shoal (SS in Fig. 1b) is co-located with SSTS with monthly records available; we examine monthly data from this site for seasonal sea-level changes. We obtained hourly records at TP from the University of Hawaii Sea Level Centre (Caldwell et al. 2015), monthly records at SS from the Permanent Service for Mean Sea Level (Holgate et al. 2013), and reprocessed multi-mission altimetric gridded sea-level anomaly (SLA) with daily temporal resolution and spatial sampling of 0.25 degree from the Copernicus Climate Change Service (C3S). Various geophysical corrections, including dynamic atmospheric corrections that account for variations in sea level due to a low-frequency inverse barometer response and high-frequency wind and pressure effects (Carrere et al. 2016), were applied to the gridded SLA products (Taburet et al. 2019).

GNSS SNR data analysis to retrieve sea levels

We used GPS and GLONASS satellite signals for retrieving sea levels. Figure 2 shows the reflection areas that can be sensed by the two GNSS antennas at SNSC and SSTS. As both stations were originally installed for serving the needs of survey and mapping applications, they are not at optimal locations for sea-level monitoring. The view of the water from the two stations is limited, and to avoid including reflections from the land we must define an azimuth and elevation angle mask. For SNSC, we choose data with elevation angles between 5° and 15°. Azimuthally, the location of this particular site allows data from only 150°–260°. For SSTS, we apply a mask of elevation angle between 5 and 15°, and restrict azimuths to between −100 and 60°. The GPS/GLONASS satellite tracks shown in Fig. 2 are those after the mask has been applied. We first generate reflector height time series H_G and H_R from GPS and GLONASS SNR data, respectively. Second, we convert reflector heights to relative sea levels $h_G = -\left(H_G - \overline{H}_G\right)$ and $h_R = -\left(H_R - \overline{H}_R\right)$. Finally, we combine h_G and h_R to form sea-level time series h_{GNSS} for the subsequent analysis of tides and seasonal cycles.

Tidal harmonic analysis

We used the MATLAB Unified Tidal Analysis and Prediction (Utide) software package to perform tidal harmonic analysis (Codiga 2011). The analysis function accepts records with times that are uniformly or irregularly distributed, satisfying the needs of both tide-gauge records and GNSS-IR measurements; tide-gauge records are uniformly hourly data, whereas sea-level observations generated from GNSS-IR are not evenly sampled. We configured Utide for iteratively re-weighted least-squares to harmonically estimate automatically selected

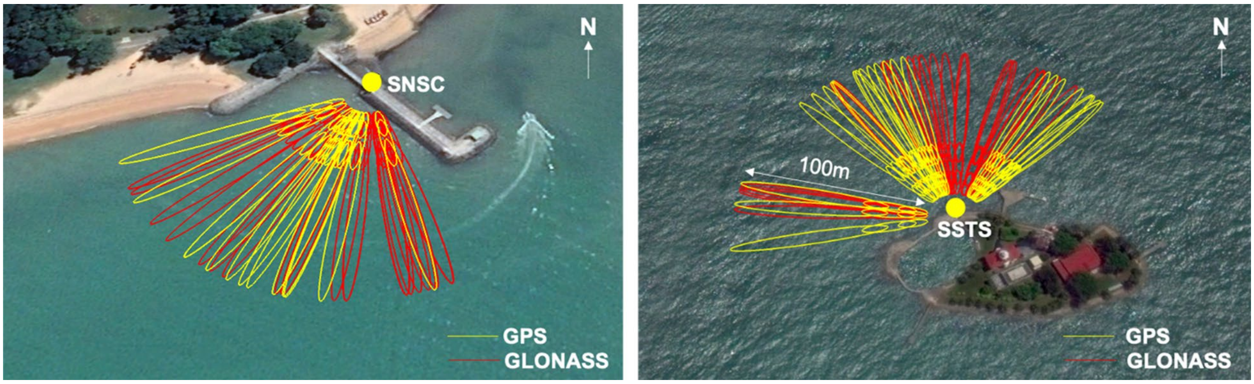

Fig. 2 Locations of the two GNSS sites SNSC and SSTS (yellow dots), and the corresponding reflection areas (red and yellow ellipses), which were approximated by the first Fresnel zone for a reflector height of 5 m for both SNSC and SSTS, respectively. The ellipses for each satellite track are the sensing zones for GPS/GLONASS observations for elevation angles 5° (longest ellipse), 8° (second ellipse), and 15° (shortest ellipse). The sensing zones in the figure were calculated at L1 frequency. We made the figures using Google Earth

constituents and spectra of actual residuals in the computation of confidence intervals.

Results

Individual sea-level estimates

At SNSC, the number of daily sea-level measurements from GPS (L1–C/A) and GLONASS (L1C) combined is between 31 and 51 with a median of 45; and the corresponding time between successive measurements is between 5 to 160 min with a median of 25 min (Fig. 3). At SSTS, the median of number of daily measurements is 47, and the median of time between successive measurements is 23 min (Fig. 4).

The tide gauge at TP is located in-between the two GNSS stations. SNSC is situated in the east, ~ 14 km away, whereas SSTS is in the west at a distance of ~ 23 km. We match each sea-level estimate from GNSS SNR data h_{GNSS} with a corresponding tide-gauge value h_{TG} by linearly interpolating hourly tide-gauge records in time. For both time series we subtracted the mean and then used the residuals to form a time series of differences,

$$\Delta h = h_{\text{TG}} - h_{\text{GNSS}}$$

To evaluate whether sea levels at SSTS and SNSC can be compared with tide-gauge records at TP, we computed a two-dimensional density of the corresponding pairs $(\Delta h, h_{\text{TG}})$ for the entire analysis period and displayed the

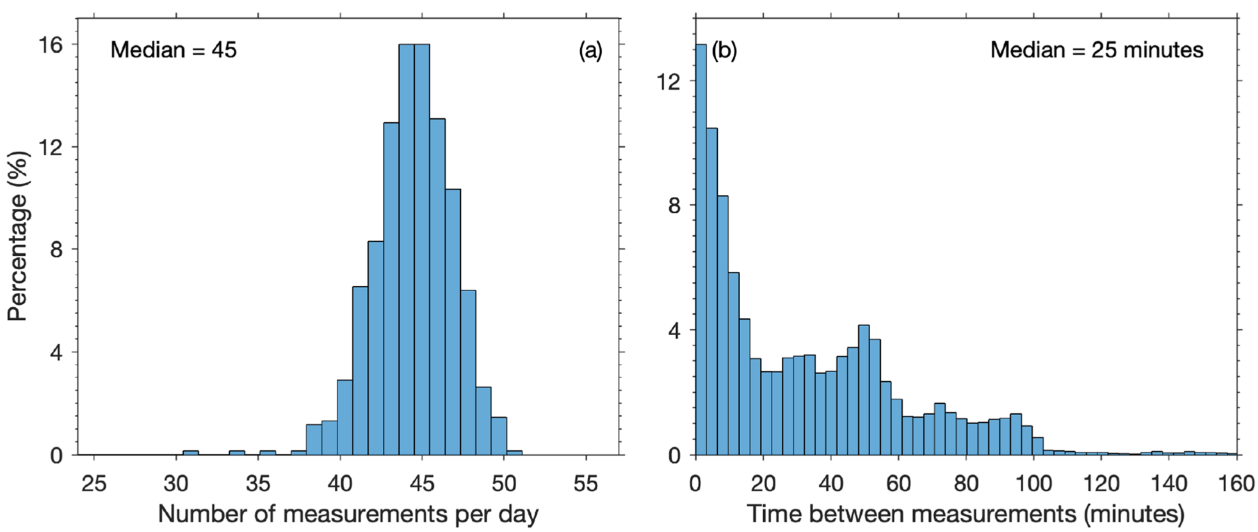

Fig. 3 **a** Histogram of the number of sea level estimates from GPS (L1–C/A) and GLONASS (L1C) combined each day over the 3-year period from 2017 to 2019 at SNSC. **b** Histogram of time (min) between successive GNSS sea level estimates

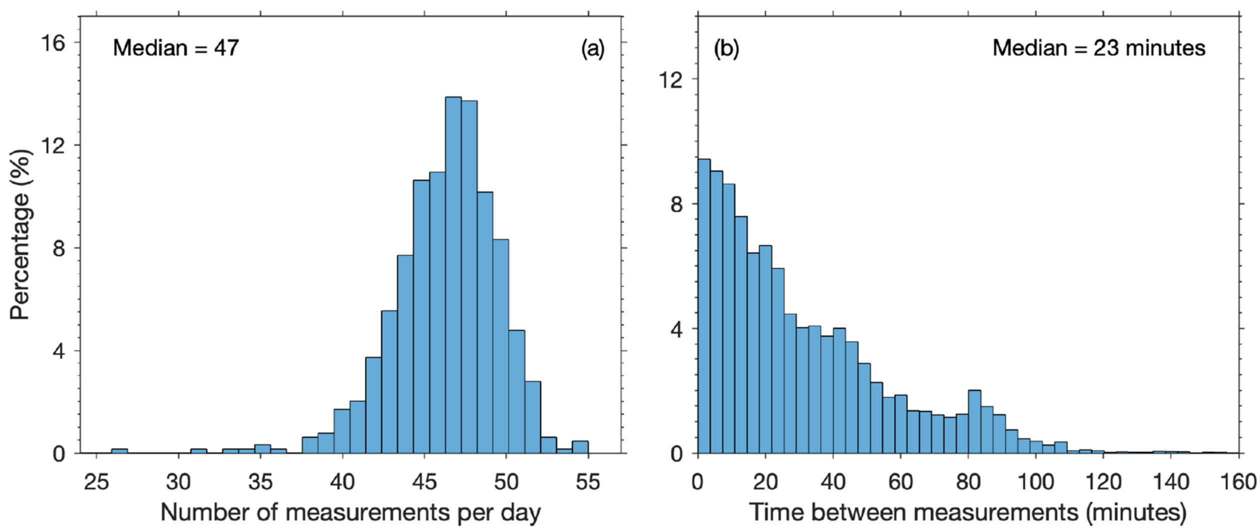

Fig. 4 Same as Fig. 3, but for SSTS

differences between the measurements from tide gauge and GNSS at SSTS and SNSC on a Van de Casteele diagram (Martin Miguez et al. 2008), shown in Fig. 5. The diagram has been found useful for comparison tests of tide gauges, since it can indicate scale problems, time-keeping errors and other issues (Pérez et al. 2014). Figure 5a shows that the differences between TP and SSTS are due to a time shift. Since the Singapore Strait is in a sharp transition zone and the two sites are 23 km apart, the time shift most likely reflects a real difference in tidal dynamics. Hence, sea-level measurements at SSTS cannot be directly compared with tide-gauge records at TP.

Figure 5b shows that, between measurements at TP and SNSC, for $h > 0$, Δh is slightly skewed toward positive values; and for $h < 0$, Δh is slightly skewed toward negative values, indicating that a scale difference may exist. Therefore, we computed a linear fit between the two time series

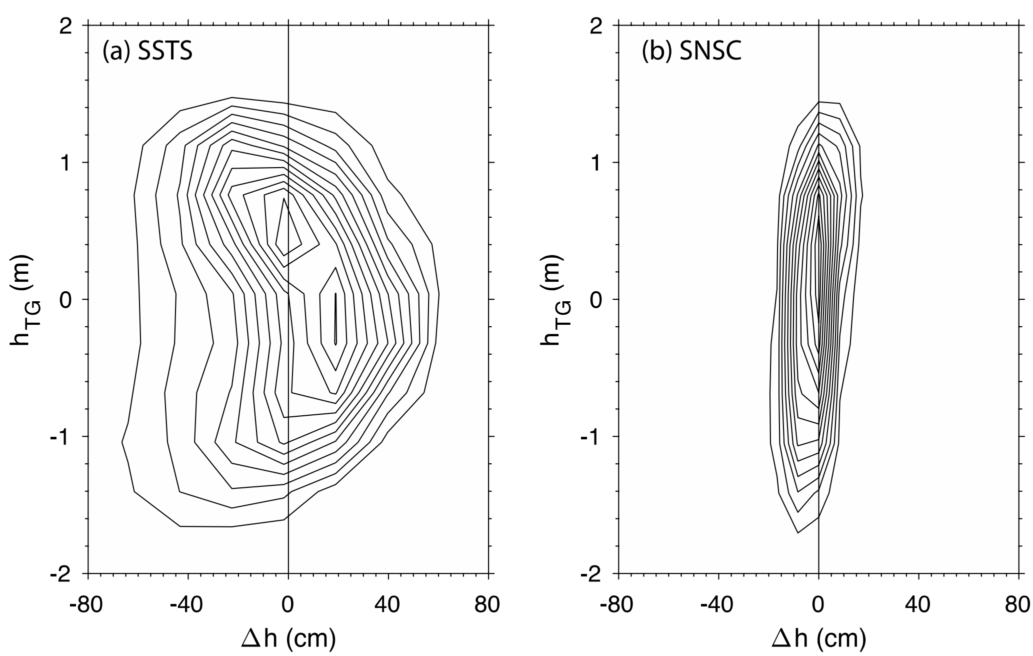

Fig. 5 Van de Casteele diagram as a two-dimensional density of the differences Δh between the GNSS (GPS L1–C/A and GLONASS L1C) and tide-gauge sea level measurements as a function of the sea level h_{TG}. Contour levels are linear, in arbitrary units. The mean of h is set to zero

$$h_{\mathrm{GNSS}} = \alpha h_{\mathrm{TG}} + c$$

From this we found $\alpha = 1.0269 \pm 0.0007$, suggesting a scale difference of 2.7%. As the two sites are not exactly co-located, the observed discrepancies could be due to instrumentation or to real changes in the tidal ranges (see further discussion in "Tides"). Still, the scale difference is smaller than corresponding differences between different types of tide gauges found by Pérez et al. (2014). Among their 17 pairs of gauges, they found the largest scale difference of 7.9% between two sensors which are 2.5 km apart and interpreted it as a consequence of the difference in seasonal cycle due to a pressure sensor affected by seasonal variations in seawater density. We, therefore, conclude that tide-gauge records at TP can be directly compared with sea-level measurements at SNSC generated from GNSS-IR. The root-mean-square deviation (RMSD) of the differences between tide-gauge records at TP and GNSS-based sea-level estimates at SNSC is 7.1 cm, suggesting that sea levels at TP and SNSC agree reasonably well despite the distance (14 km) between the two locations.

Tides

High temporal resolution of sea level is critical for tidal harmonic analysis, usually requiring hourly or higher frequency observations (Crawford 1995). At SNSC and SSTS, sea-level measurements from individual GNSS signals are at relatively low temporal resolutions, and they are not uniformly sampled in time. Therefore, we used the combined sea-level estimates from GPS L1–C/A and GLONASS L1C signals to conduct tidal harmonic analysis. We chose to combine sea levels from those two signals as they slightly outperform GPS L2C and GLONASS L2C signals in terms of both the number of observations and RMSD differences with tide-gauge records.

To identify the tides type at the three locations, we calculated form factors F based on the estimated amplitudes in Table 1. They are 0.55, 0.54 and 0.40 at SNSC, TP and SSTS, respectively, indicating that tides at the three locations are all in mixed, mainly semi-diurnal form. Haigh et al. (2011) demonstrated that estimation of tidal ranges at locations with tides in mixed or diurnal form can be simplified as the difference between mean higher-high water ($\mathrm{MHHW} = A_{M_2} + A_{O_1} + A_{K_1}$) and mean lower-low water ($\mathrm{MLLW} = -A_{M_2} - A_{O_1} - A_{K_1}$). We thus adopted the simplified method to compute tidal ranges at the three locations and found that they are 2.7 m at SNSC, 2.8 m at TP and 2.8 m at SSTS. Tidal ranges at SNSC and TP are slightly different, suggesting that the scale difference demonstrated in "Individual sea-level estimates" section is a reflection of a change of tidal environment at the two sites.

Our results show that at the three locations M_2 is the largest tidal constituent, followed by S_2, K_1 and O_1. Geographically, the amplitudes of the two principal semi-diurnal constituents M_2 and S_2 gradually increase toward the west, i.e., the amplitudes at SNSC are smaller than

Table 1 Summary of harmonic analysis results for the eight major tidal constituents and selected shallow-water tidal constituents

Tidal constituent	Amplitude (cm)			Phase (degree)		
	SNSC	TP	SSTS	SNSC	TP	SSTS
Eight major tidal constituents						
M_2	75.6 ± 0.1	80.2 ± 0.1	85.4 ± 0.1	90.7 ± 0.1	91.5 ± 0.1	101.4 ± 0.1
S_2	29.9 ± 0.1	32.4 ± 0.1	38.4 ± 0.2	137.2 ± 0.2	137.4 ± 0.2	147.0 ± 0.2
N_2	14.8 ± 0.1	15.8 ± 0.1	15.7 ± 0.1	69.3 ± 0.5	72.0 ± 0.4	87.1 ± 0.6
K_2	10.6 ± 0.1	9.7 ± 0.1	10.9 ± 0.2	135.6 ± 0.5	138.8 ± 0.7	144.0 ± 0.7
K_1	28.9 ± 0.1	30.6 ± 0.1	26.4 ± 0.1	346.8 ± 0.2	352.3 ± 0.2	36.1 + 0.2
O_1	28.8 ± 0.1	29.5 ± 0.1	23.1 ± 0.1	302.2 ± 0.2	307.4 ± 0.2	351.6 + 0.3
P_1	9.1 ± 0.1	9.4 ± 0.1	7.7 ± 0.1	339.2 + 0.7	343.9 ± 0.7	28.5 ± 1.0
Q_1	6.5 ± 0.1	6.6 ± 0.1	4.5 ± 0.1	271.8 ± 1.1	276.3 ± 0.9	319.1 ± 1.4
Selected shallow water tidal constituents						
M_4	1.3 ± 0.1	1.5 ± 0.1	4.1 ± 0.1	211.3 ± 3.4	192.6 ± 2.7	147.8 ± 1.4
MS_4	1.2 ± 0.1	1.7 ± 0.1	3.9 ± 0.1	234.9 ± 3.1	222.6 ± 2.2	187.7 ± 1.3
MK_3	1.8 ± 0.1	1.9 ± 0.1	3.2 ± 0.1	96.9 ± 2.6	105.2 ± 2.6	68.6 ± 1.5
SO_3	1.5 ± 0.1	1.7 ± 0.1	2.6 ± 0.1	122.9 ± 2.9	128.3 ± 2.9	86.3 ± 2.0
MO_3	1.3 ± 0.1	1.6 ± 0.1	2.5 ± 0.1	61.2 ± 3.2	71.8 ± 2.8	34.6 ± 1.8
$2MS_6$	1.4 ± 0.1	1.6 ± 0.1	2.1 ± 0.1	193.4 ± 3.1	186.8 ± 1.2	153.9 ± 1.7
MK_4	1.0 ± 0.1	1.1 ± 0.1	1.5 ± 0.1	186.7 ± 4.3	194.0 ± 3.9	185.6 ± 3.8

The uncertainties indicate 95% confidence level based on colored noise those at TP, and those at TP are less significant than those at SSTS, whereas the amplitudes of the two principal diurnal constituents K_1 and O_1 overall decrease westwardly. This is anticipated as the Singapore Strait is located in an exceptionally sharp transition zone, where the dominantly diurnal tides change into semidiurnal tides within a distance of 400 km. The transition from diurnal to semidiurnal is the result of an increase of M_2 amplitude and a decrease in diurnal amplitudes (Van Maren and Gerritsen 2012).

In addition, O_1 amplitudes at SNSC and TP are comparable within the 95% confidence level; however, the K_1 amplitude at SNSC is slightly smaller (1.7 cm) than that at TP, even though it is anticipated to be comparable or slightly greater. Possible causes could be errors in the GNSS-IR estimate due to the geometrical errors caused by the GPS orbital periods coinciding with K_1 and K_2 periods and/or errors in the tide gauge due to inadequately compensated changes in the temperature within the acoustic sound channel. Tabibi et al. (2020) revealed that the K_1 and K_2 amplitudes estimated from GPS SNR data show systematic errors (around 1.1 cm compared with co-located tide-gauge results) due to GPS geometrical errors. In addition, Larson et al. (2017) found a discrepancy of 1 cm in the S_1 amplitudes estimated using data from an acoustic tide gauge and a GPS, and attributed the discrepancy to errors in the tide gauge, because the S_1 frequency is coincident with the mean daily heating and cooling cycle; thermal effects are a known error source in the acoustic tide gauges but likely to be small in the GNSS instrumentation. They also hypothesized that similar errors could arise at K_1 and P_1, because both frequencies are 1 cycle per day from the S_1 frequency.

Table 1 also shows that phases of the eight major tidal constituents at SNSC and TP are overall similar, but phases at SSTS are significantly different from those at TP, further proving that sea levels at SSTS and TP are not comparable.

Tidal asymmetry

In shallow coastal waters, energy from the dominant fundamental tidal constituents is transferred non-linearly through processes including advection, finite-amplitude effects and friction, generating higher frequency harmonic overtides (e.g., M_4, originated from M_2) and compound tides (e.g., MK_3, from the combination of M_2 and K_1) (Jewell et al. 2012). Tidal asymmetry can become much stronger due to the generation of shallow water overtides and compound tides in shallow coastal areas with tides dominated by M_2. We show shallow water tidal constituents with amplitudes greater than 1 cm at all three locations in Table 1. In general, amplitudes of those shallow water tidal constituents increase from SNSC to TP and then to SSTS, which may indicate a stronger tidal asymmetry westwardly in the Singapore Strait.

Harmonic and statistical methods are the two commonly used methods to quantify tidal asymmetry due to the unequal durations of rising and falling tides (also referred to as tidal duration asymmetry). Guo et al. (2019) demonstrated that both harmonic and statistical methods are effective in indicating tidal asymmetry. In this study, we adopt the skewness method, which is based on harmonic amplitudes, phases and frequencies, proposed by Song et al. (2011) to quantify tidal duration asymmetry. We adopt this method, because it can be used to understand the asymmetries of tidal records regardless of the tidal regime (diurnal, mixed or semi-diurnal) or the constituents that dominate the asymmetry.

We first identify the constituents responsible for asymmetry by exploring all the possible combinations of pairs and triples of constituents that contribute to skewness; that is, the constituents for which the following frequency ratios—$2\omega_1 = \omega_2$ and $\omega_1 + \omega_2 = \omega_3$—are met. In total, 342 combinations of pairs and triples of tidal constituents could produce skewness. We then calculate the contribution of each combination to skewness β_i via Eqs. (17) and (18) and the total tidal skewness γ_N via Eq. (22) in Song et al. (2011). If $\gamma_N > 0$, the tidal distribution is positively asymmetric, which implies that the duration of rising tide is shorter, i.e., flood dominant tidal asymmetry. If $\gamma_N < 0$, the tidal distribution is negatively asymmetric, implying that the duration of falling tide is shorter, i.e., ebb dominant tidal asymmetry. Typically, the tidal asymmetry is considered to be significant if $|\gamma_N| > 0.1$.

Table 2 displays the total tidal skewness γ_N and the three largest combinations of tidal constituents that produce skewness β_i. At the three locations, the tidal asymmetry is pronounced at SSTS, and the major contribution to asymmetry is the combination of M_2, S_2 and MS_4 constituents, indicating that tidal wave distortion and

Table 2 Summary of the total asymmetry via Skewness and three major combinations and their contributions to γ_N

Station	γ_N	Combination 1	β_1	Combination 2	β_2	Combination 3	β_3
SNSC	−0.047	$O_1/K_1/M_2$	−0.032	$M_2/S_2/MS_4$	−0.009	$M_2/K_2/MK_4$	0.007
TP	−0.056	$O_1/K_1/M_2$	−0.045	$M_2/O_1/MO_3$	−0.007	$M_2/K_2/MK_4$	0.006
SSTS	0.1589	$M_2/S_2/MS_4$	0.1020	$O_1/K_1/M_2$	−0.054	$M_2/K_1/MK_3$	0.022

asymmetry is mainly originated from non-linear interaction of tides and the geometry of shoreline and/or shallow water depth as compound tide MS_4 (non-linear interaction of M_2 and S_2) is involved in the abovementioned combination. In addition, γ_N is positive at SSTS, indicating a flood dominant tidal asymmetry (i.e., the duration of the rising tide is shorter). Numerical modelling in the Singapore Strait from Maren and Gerritsen (2012) did not reveal such asymmetry as only the eight major tidal constituents and a mean cycle of the monsoon-induced water level were included in the simulation.

Compared to SSTS, the tidal asymmetry at SNSC and TP is less significant and ebb dominant, and the combination of O_1, K_1 and M_2 constituents is the main source of tidal asymmetry by astronomical forcing. This is in line with the findings by Van Maren and Gerritsen (2012) who, based on the analysis of tides in the Singapore Strait from numerical modelling, concluded that the asymmetry of the tides results from the inclination of O_1, K_1 and M_2 constituents.

Annual cycle

We noted an amplitude of >6 cm in the annual constituents (S_a) from the tidal harmonic analysis. Ray et al. (2021) showed that the astronomical tidal forcing S_a constituents along the equator are < 2.5 mm; therefore, those annual changes in sea level are driven by meteorological tide. To quantify the meteorological effects on annual sea-level changes in the Singapore Strait, we supplement measurements from GNSS-IR with data from tide gauges and satellite altimetry. We selected the grid points of the satellite altimetry products that are nearest to SNSC and SSTS (G1 and G2 in Fig. 1a). Note that we added the dynamic atmospheric corrections back to the sea level anomalies produced by C3S.

We first removed tidal effects and then calculated daily means of sea-level measurements at SNSC and SSTS (GNSS-IR) and at TP (tide gauge). Details of how we carried out the daily mean calculations can be found in Peng et al. (2021). In addition, we filtered out high-frequency signals with periods < 2 months by applying a 59-day moving average to daily means of sea-level measurements from GNSS-IR, tide gauge and satellite altimetry.

Figures 6 and 7 show that annual sea-level changes are the dominant seasonal signal at the GNSS and tide gauge stations, and at G1 and G2 from satellite altimetry. Annually, sea levels at those sites peak in November/December and reach the lowest in June/July, consistent with the findings from Tkalich et al. (2013a), who demonstrated that sea-level anomalies in the Singapore Strait are at the highest during November to February due to the Northeast monsoon, and conversely at the lowest during June to August due to the Southwest monsoon.

To estimate amplitudes of annual sea-level changes, we employ a common least squares approach to fit the data with a model including annual harmonics, a rate, and an offset. Our results show that the annual amplitudes are 13.6 cm at SNSC and TP, and 13.9 cm at G1. At SSTS, SS and G2, annual amplitudes are 6.7 cm, 7.0 cm, and 7.2 cm, respectively. Uncertainties in the estimated amplitudes are about 0.1 cm from daily means and 0.8 cm from the monthly average (i.e., tide-gauge records at SS). Overall, the amplitudes at SNSC and TP agree well with that from satellite altimetry at G1, and the amplitudes

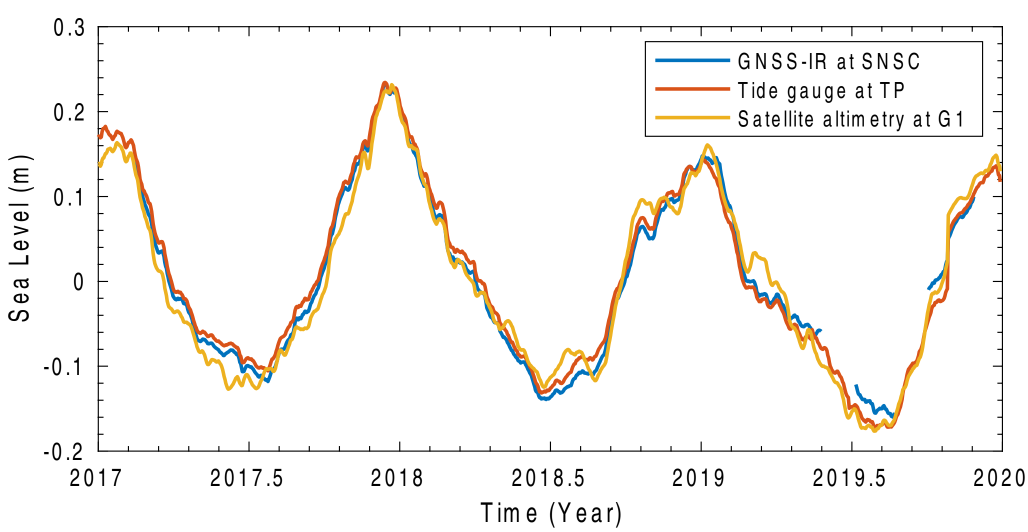

Fig. 6 Daily means of sea-level measurements at SNSC from GNSS-IR, at TP from tide gauge and at G1 from satellite altimetry. The measurements from these three different observing systems agree well

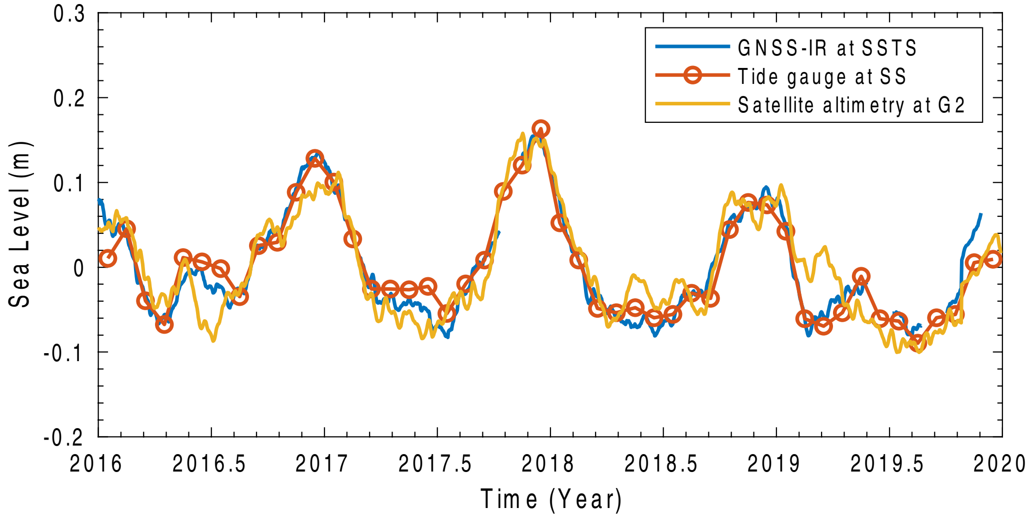

Fig. 7 Same as Fig. 6, but for SSTS. The tide-gauge data at SS are monthly records

at SSTS, SS and G2 are in good agreement. However, annual amplitudes at SNSC, TP and G1 are greater than those estimated from SSTS, SS and G1. This discrepancy in amplitudes can be explained by the locations they are situated at. Tkalich et al. (2013b) and Tay et al. (2016) revealed that the most significant factor that determines variability in sea-level anomalies in the Singapore Straits is the wind over the central part of the South China Sea. SSTS, SS and G2 are in the west of the Singapore Strait, nearer to the Indian Ocean, where they are more shielded from the monsoon climatological effects, thus experiencing weaker seasonal signals. On the contrary, SNSC, TP, and G1 are in the east of the Singapore Strait and nearer to the South China Sea; consequently, they experience more prominent signals, since they are more exposed to the monsoon effects.

It should be noted that sea levels at G1 and G2 do not perfectly match those at SNSC and SSTS, one possible reason could be modulation of atmospheric forcing such as Indian Ocean dipole and El Niño–Southern Oscillation at interannual timescales, and their contributions vary in different locations (Tay et al. 2016). However, addressing the interannual variability of sea level is beyond the scope of this study as the record length (3–4 years) is not adequately long.

Conclusions and discussion

From tidal harmonic analysis of 3 years of GNSS-IR sea-level measurements at SNSC and SSTS, and 3 years of hourly tide-gauge records at TP, we found that tidal regimes at the three sites are all mixed and mainly semi-diurnal. We also observed an increase of M_2 and S_2 (the two principle semi-diurnal constituents) amplitudes westwardly and a decrease of K_1 and O_1 (the two principle diurnal constituents) amplitudes. This demonstrates that GNSS-IR captured the tidal transition in the Singapore Strait. The transition also results in a decrease of tidal form factors toward the west in the Singapore Strait, but the overall tidal ranges at the three locations are at a similar level of 2.7 m to 2.8 m. We also used a harmonic-based skewness method to quantify the tidal duration asymmetry and found that the tide at station SSTS is positively asymmetric (i.e., flood dominant), whereas the tidal asymmetry at SNSC and TP is less significant and ebb dominant. Non-linear interaction of major tidal constituents is the main cause of tidal asymmetry at SSTS, whereas the combination of $O_1/K_1/M_2$ is the major contribution to the asymmetry by astronomical forcing at SNSC and TP.

By examining data from GNSS-IR, tide gauge and satellite altimetry, we inferred that monsoon winds flowing from the central South China Sea greatly impact the seasonal sea-level changes in the Singapore Strait: the annual amplitude at SNSC is 13.6 cm, twice the amplitude at SSTS, which is 6.7 cm. This is due to the locations of the two sites. The eastern side of the Singapore Strait is in connection with the South China Sea, which is located in the southwest-northeast pathway of Asian monsoons, therefore, experiencing stronger winds compared with the western side of the Singapore Strait, consequently resulting in a higher annual amplitude in sea-level changes.

Due to the shallow and strongly varying water depth, irregular shorelines, complex tidal regime and seasonal monsoon winds in the Singapore Strait, numerical modelling of tides in this region is particularly difficult and could be biased (Hasan et al. 2016). Assimilating GNSS-IR sea-level observations in the modeling may potentially improve the performance of global and regional tidal models in the region.

We plan to install more GNSS stations in Singapore for measuring sea surface height and land height. Their antennas will be configured to track all the GNSS satellites (GPS, GLONASS, BeiDou, Galileo, and QZSS). We anticipate further improvement in temporal resolution of sea-level estimates from GNSS-IR with contributions from Galileo. Data from those stations will be used to study tides and monsoon effects on the sea surface heights. For the long term they can be used to separate contributions from land-height change and climate-induced sea surface height changes, as coastal GNSS can simultaneously provide continuous weather-independent sea-level information and vertical land motions.

Supplementary Information

The online version contains supplementary material available at https://doi.org/10.1186/s40562-023-00294-7.

Additional file 1. Additional texts: **Texts S1** to **S4**; additional figures: **Figures S1** to **S4**; and additional tables: **Tables S1** to **S3**.

Acknowledgements
We thank the reviewers and editors for their valuable comments which helped to improve the manuscript. This work comprises Earth Observatory of Singapore contribution 532.

Author contributions
Conceptualization: DP; data curation: EM and PWW; formal analysis: DP and KYS; funding acquisition: EMH; investigation: DP and KYS; methodology: DP; project administration: EMH and VHSK; resources: VHSK, EM and PWW; writing—original draft: DP; writing—review and editing: KYS, VHSK, EM, and EMH.

Funding
This research was supported by Singapore Ministry of Education Academic Research Fund Tier 3 (MOE 2019-T3-1-004), and by the National Research Foundation Singapore under its NRF Investigatorship scheme (National Research Investigatorship Award No. NRF-NRFI05-2019-0009), the Earth Observatory of Singapore (EOS), the National Research Foundation of Singapore, and the Singapore Ministry of Education under the Research Centers of Excellence initiative. This research is also supported by the NRF, Singapore, and National Environment Agency, Singapore under the National Sea Level Programme Initiative as part of the Urban Solutions and Sustainability—Integration Fund (Award No. USS-IF-2020-5) by a grant (Proposal ID NSLP-2021-3R-05) awarded to E.M.H.

Availability of data and materials
Sea level estimates derived from GPS and GLONASS SNR data in this study can be downloaded from DR-NTU (data) https://doi.org/10.21979/N9/JKB5QY. We obtained hourly tide-gauge records from the University of Hawaii Sea Level Center (https://uhslc.soest.hawaii.edu/) and monthly tide-gauge records from the Permanent Service for the Mean Sea Level (https://www.psmsl.org/). Satellite altimetry data are freely available at the Copernicus Marine Environment Monitoring Service: https://marine.copernicus.eu/. Dynamic atmospheric corrections are available at Aviso+: https://www.aviso.altimetry.fr/en/home.html.

Declarations

Competing interests
The authors declare that they have no competing interests.

Received: 6 March 2023 Accepted: 20 August 2023
Published online: 25 August 2023

References
Caldwell P, Merrifield M, Thompson P (2015) Sea level measured by tide gauges from global oceans–the Joint Archive for Sea Level holdings (NCEI Accession 0019568), Version 5.5, NOAA National Centers for Environmental Information, Dataset. Centers Environ. Information, Dataset, 10, V5V40S47W

Carrere L, Faugère Y, Ablain M (2016) Major improvement of altimetry sea level estimations using pressure-derived corrections based on ERA-Interim atmospheric reanalysis. Ocean Sci 12(3):825–842

Codiga DL (2011) Unified tidal analysis and prediction using the UTide Matlab functions. Technical Report 2011–01. Graduate School of Oceanography, University of Rhode Island, Narragansett, RI. 59pp. ftp://www.po.gso.uri.edu/pub/downloads/codiga/pubs/2011Codiga-UTide-Report.pdf

Collins DS, Avdis A, Allison PA, Johnson HD, Hill J, Piggott MD, Hassan MHA, Damit AR (2017) Tidal dynamics and mangrove carbon sequestration during the Oligo-Miocene in the South China Sea. Nat Commun 8(1):1–12

Crawford WR (1995) A technique for quality control and selection of tidal harmonic constituents. The International Hydrographic Review

De Swart H, Zimmerman J (2009) Morphodynamics of tidal inlet systems. Annu Rev Fluid Mech 41:203–229

Guo L, Wang ZB, Townend I, He Q (2019) Quantification of tidal asymmetry and its nonstationary variations. J Geophys Res Oceans 124(1):773–787. https://doi.org/10.1029/2018jc014372

Haigh ID, Eliot M, Pattiaratchi C (2011) Global influences of the 18.61 year nodal cycle and 8.85 year cycle of lunar perigee on high tidal levels. J Geophys Res Oceans. https://doi.org/10.1029/2010JC006645

Hasan GJ, van Maren DS, Ooi SK (2016) Hydrodynamic modeling of Singapore's coastal waters: nesting and model accuracy. Ocean Model 97:141–151

Holgate SJ, Matthews A, Woodworth PL, Rickards LJ, Tamisiea ME, Bradshaw E, Foden PR, Gordon KM, Jevrejeva S, Pugh J (2013) New data systems and products at the permanent service for mean sea level. J Coastal Res 29(3):493–504

Jewell SA, Walker DJ, Fortunato AB (2012) Tidal asymmetry in a coastal lagoon subject to a mixed tidal regime. Geomorphology 138(1):171–180

Jin S, Qian X, Wu X (2017) Sea level change from BeiDou Navigation Satellite System-Reflectometry (BDS-R): first results and evaluation. Global Planet Change 149:20–25

Larson KM, Löfgren JS, Haas R (2013) Coastal sea level measurements using a single geodetic GPS receiver. Adv Space Res 51(8):1301–1310

Larson KM, Ray RD, Williams SD (2017) A 10-year comparison of water levels measured with a geodetic GPS receiver versus a conventional tide gauge. J Atmos Oceanic Tech 34(2):295–307

Mandal S, Sil S, Gangopadhyay A, Jena BK, Venkatesan R (2020) On the nature of tidal asymmetry in the Gulf of Khambhat, Arabian Sea using HF radar surface currents. Estuar Coast Shelf Sci 232:106481

Martin Miguez B, Testut L, Wöppelmann G (2008) The Van de Casteele test revisited: an efficient approach to tide gauge error characterization. J Atmos Oceanic Tech 25(7):1238–1244. https://doi.org/10.1175/2007jtecho554.1

Mitra A, Kumar VS (2021) A numerical investigation on the tide-induced residence time and its association with the suspended sediment concentration in Gulf of Khambhat, northern Arabian Sea. Mar Pollut Bull 163:111947

Molinas E, Carneiro JC, Vinzon S (2020) Internal tides as a major process in Amazon continental shelf fine sediment transport. Mar Geol 430:106360

Nidzieko NJ (2010) Tidal asymmetry in estuaries with mixed semidiurnal/diurnal tides. J Geophys Res Oceans. https://doi.org/10.1029/2009JC005864

Olliver EA, Edmonds D, Shaw J (2020) Influence of floods, tides, and vegetation on sediment retention in Wax Lake Delta, Louisiana, USA. J Geophys Res Earth Surf 125(1):e2019JF005316
Peng D, Larson KM, Feng L, Hill EM (2021) Measuring coastal absolute sea-level change using GNSS interferometric reflectometru. Remote Sens 13(21):4319
Pérez B, Payo A, López D, Woodworth P, Alvarez Fanjul E (2014) Overlapping sea level time series measured using different technologies: an example from the REDMAR Spanish network. Nat Hazard 14(3):589–610
Pugh D, Woodworth P (2014) Sea-level science: understanding tides, surges, tsunamis and mean sea-level changes. Cambridge University Press
Ray RD, Loomis BD, Zlotnicki V (2021) The mean seasonal cycle in relative sea level from satellite altimetry and gravimetry. J Geodesy 95(7):1–21
Song D, Wang XH, Kiss AE, Bao X (2011) The contribution to tidal asymmetry by different combinations of tidal constituents. J Geophys Res Oceans. https://doi.org/10.1029/2011JC007270
Tabibi S, Geremia-Nievinski F, Francis O, van Dam T (2020) Tidal analysis of GNSS reflectometry applied for coastal sea level sensing in Antarctica and Greenland. Remote Sens Environ 248:111959
Taburet G, Sanchez-Roman A, Ballarotta M, Pujol M-I, Legeais J-F, Fournier F, Faugere Y, Dibarboure G (2019) DUACS DT2018: 25 years of reprocessed sea level altimetry products. Ocean Sci 15(5):1207–1224
Tay SHX, Kurniawan A, Ooi SK, Babovic V (2016) Sea level anomalies in straits of Malacca and Singapore. Appl Ocean Res 58:104–117
Tkalich P, Vethamony P, Babu M, Malanotte-Rizzoli P (2013a) Storm surges in the Singapore Strait due to winds in the South China Sea. Nat Hazards 66(3):1345–1362
Tkalich P, Vethamony P, Luu Q-H, Babu M (2013b) Sea level trend and variability in the Singapore Strait. Ocean Sci 9(2):293–300
Van Maren D, Gerritsen H (2012) Residual flow and tidal asymmetry in the Singapore Strait, with implications for resuspension and residual transport of sediment. J Geophys Res Oceans. https://doi.org/10.1029/2011JC007615
Vousdoukas MI, Ranasinghe R, Mentaschi L, Plomaritis TA, Athanasiou P, Luijendijk A, Feyen L (2020) Sandy coastlines under threat of erosion. Nat Clim Chang 10(3):260–263

Publisher's Note